

INFRARED IMAGING USING MICROCANTILEVERS

Patrick I. Oden*, Panos G. Datskos*, Thomas G. Thundat
Eric A. Wachter, Robert J. Warmack*

Health Science Research Division
Oak Ridge National Laboratory
Oak Ridge, Tennessee

*Department of Physics and Astronomy
University of Tennessee
Knoxville, Tennessee

ABSTRACT

A micromechanical detector using microcantilever for infrared (IR) radiation is demonstrated. Because of their small size and low thermal mass, these microcantilever IR detectors are promising new family of IR sensors. This novel IR sensor is based on deflection due to IR adsorption induced thermal stress on a bimaterial cantilever which can be monitored with several methods such as optical deflection or piezoresistive. When laser-deflection-monitored Si_3N_4 microcantilevers coated with a 40nm thick coating of gold were irradiated by a low-power diode laser, the noise equivalent power and specific detectivity, NEP and D^* were found to be $173pW/\sqrt{Hz}$ and

$7.18 \times 10^8 cm\sqrt{Hz}/W$, respectively, when compensation for the laser reflectivity was made.

INTRODUCTION

The detection of infrared radiation has extensive industrial, military, and commercial applications. Presently there are several types of commercially available infrared detectors, including photomultipliers, thermopiles, pyroelectrics, bolometers, and various solid state detectors^{1,2}. Only thermopiles have a very broadband response, since it is based on conversion of absorbed thermal energy. Unfortunately, these devices generally have a large thermal mass and slow response times ($>10ms$) and, at present, cannot be reasonably manufactured as large two-dimensional detector arrays.

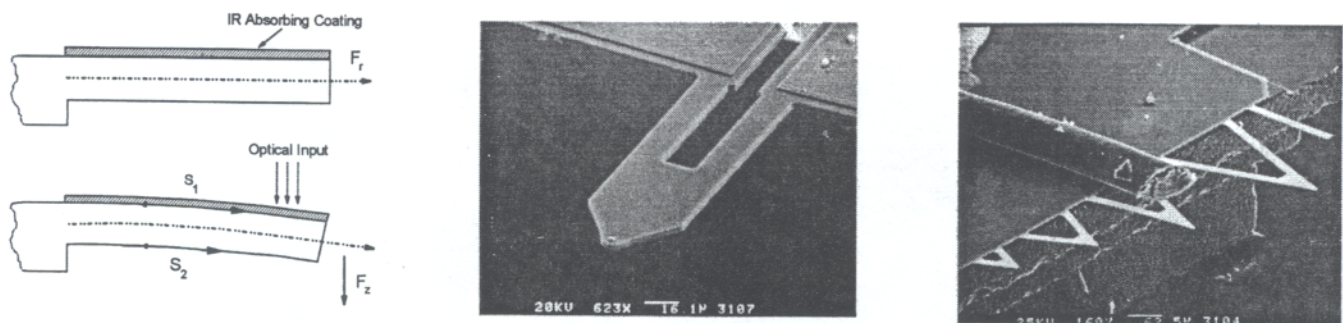


Figure 1. Left drawing is a cross-sectional schematic showing the bending response of a bimaterial cantilever with an IR adsorbing coating. Surface stresses S_1 and S_2 are balanced at equilibrium, generating a radial force F_r along the medial plane of the microcantilever. These stresses become unequal upon exposure to IR radiation producing a bending force, F_z , that displaces the tip of the microcantilever. Middle - is a scanning electron micrograph of one of the piezoelectric IR sensors used (calibration bar is $16\mu m$). Right - is another scanning electron micrograph of the Si_3N_4 microcantilevers used for the experiments compared to a human hair (calibration bar is $62.5\mu m$).

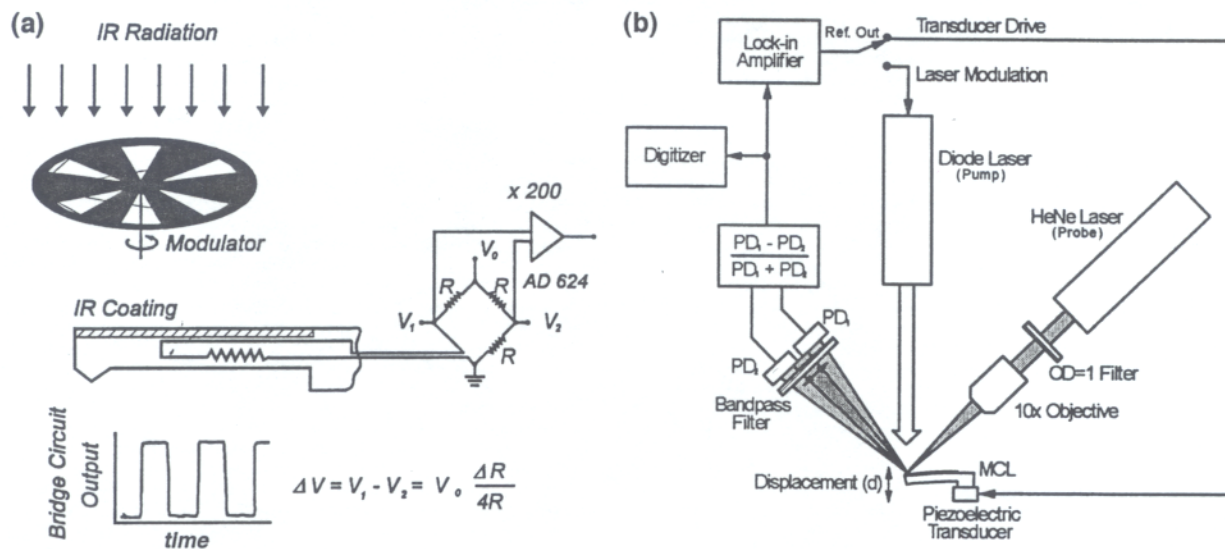


Figure 2. (a) Schematic representation of the piezoresistive IR detection experiment. The piezolever is part of a Wheatstone bridge, one of the legs connected to ground, the other to a metal film resistor with approximately the same resistance $R \sim 2000\Omega$. The other two outputs are connected to the input of a differential instrumentation amplifier. (b) Schematic diagram of the optical read-out method for IR detection.

Micromachined bolometers using suspended foils have much better rise times due to their reduced mass³. When coated with suitable optically absorbing materials both bolometers and thermopiles offers a broad spectral response. Solid state detectors for infrared radiation, such as quantum well devices, must generally be operated at reduced temperatures due to inherently high thermal noise⁴. Additionally, the spectral response of these semiconductor devices is limited by the intrinsic properties of the composing materials. Infrared detectors based on quantum detection, such as pyroelectrics, is based on conversion of incident infrared radiation into an electronic response⁵. On the other hand, infrared detection based on thermal detection, such as in bolometers and thermopiles, the IR radiation is converted into heat which is subsequently detected through temperature changes in the detector. In general, when the photon energy of the infrared radiation $h\nu > k_B T$, photon detectors offer better performance and when $h\nu < k_B T$, thermal detectors are generally favored³.

Microcantilever IR sensors provides a new approach for producing compact, light-weight, highly-sensitive micromechanical infrared detectors. This is based on the bending of a microcantilever resulting from absorption of optical energy. When a microcantilever is exposed to infrared radiation, the temperature of the cantilever increases due to absorption of this optical energy^{6,7}. If these microcantilevers are constructed from materials exhibiting dissimilar thermal expansion properties, the bimaterial effect will cause the microcantilever to bend in response to this temperature variation as shown in the left image of Figure 1.⁶⁻¹⁸ The extent of bending is directly proportional to the rate of energy absorption, which in turn is proportional to the radiation intensity. Previous work has shown that microcantilever bending can be detected with extremely high sensitivity¹⁹⁻²¹. For example, the bending of a metal-coated microcantilevers that are commonly employed in atomic force microscopy (AFM)

can be detected with sub-Angstrom ($< 10^{-10} m$) sensitivity. Recent studies have reported calorimetric detection of chemical reactions with energies as low as a few pJ based on microcantilever bending^{13,18}. It was demonstrated that the detector had an observed sensitivity of $100 pW$ corresponding to an energy of $150 fJ$ and the authors proposed using the sensor as a femtojoule calorimeter⁷. An estimate of the minimum detectable power level was of the order of $10 pW$, corresponding to a detectable energy of $20 fJ$ and a temperature sensitivity $10^{-5} K$ ⁶. The sensitivity, however, can be further improved by using an optimally designed cantilever^{6,14-17}. Therefore, an IR detector could be constructed by coating the bimaterial cantilever with appropriate absorptive materials such that they undergo bending upon exposure to infrared or near infrared radiation. These cantilevers have a typical dimension of $100-200 \mu m$ length, $0.3-4 \mu m$ thickness and $10-50 \mu m$ width. These cantilevers can be micromachined from materials such as silicon nitride, silicon or other types of semiconducting materials²². Due to the monolithic nature of these devices, they can be easily mass produced in one- and two-dimensional arrays with hundreds of levers on a single wafer.

The bending of the microcantilever is proportional to the absorbed heat energy. Assuming a spatially uniform incident power, dQ/dt , onto a bimaterial microcantilever, the maximum deflection, z_{max} , due to differential stress can be written as^{7,15,17,23}:

$$z_{max} = \frac{5}{4} \frac{(\eta_1 + \eta_2) l^3}{(\lambda_1 \eta_1 + \lambda_2 \eta_2) w t^2} \frac{(\alpha_1 - \alpha_2)(\eta dQ/dt)}{4(1 + \eta_1^2/\eta_2^2) + (6\eta_1^2 + E_1 \eta_2^2/E_2)/\eta_1 \eta_2 + E_1 \eta_1^3/E_2 \eta_2^3} \quad (1)$$

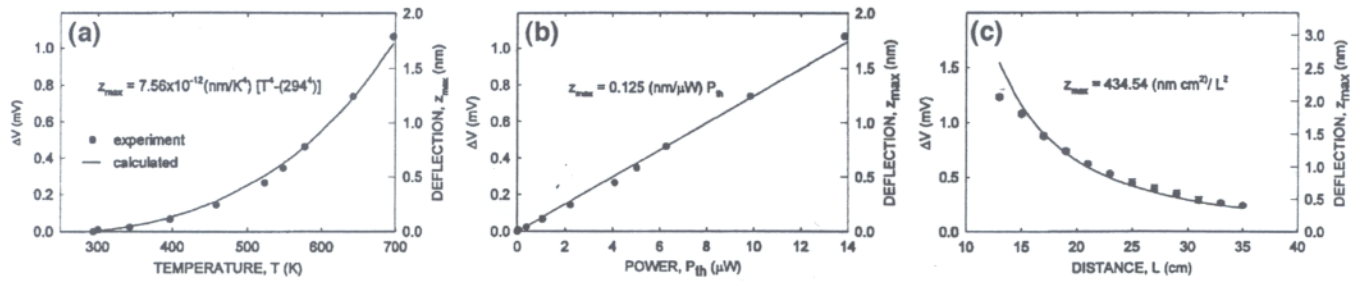


Figure 3. (a) Response of the Wheatstone bridge detection circuit, ΔV , and deflection, z_{\max} , of the piezolever as a function of the source temperature. (b) Response as a function of the absorbed thermal power and (c) as a function of IR source distance, L .

where l and w are, the length and width of the microcantilever, respectively, t_1 and t_2 are the thicknesses of the two layers, λ_1, λ_2 ; α_1, α_2 ; E_1, E_2 are the thermal conductivities; thermal expansion coefficients and Young's moduli of elasticity of the two layers; $\eta dQ/dt$ is the fraction of the radiation power absorbed.

EXPERIMENTAL

Piezoresistive Deflection Monitoring

Figure 2a shows a schematic diagram of the piezoresistive cantilever deflection detection technique. In this example, surface doped silicon microcantilevers were used in which the piezoresistance across the cantilever varied when it bent due to thermal stimulation. The design and construction of these cantilevers is described in detail elsewhere^{24,25}. The total resistance of the cantilever was approximately 2000Ω , which was electrically connected across one arm of a dc-biased Wheatstone bridge circuit and then through an Analog Devices AD 624 instrumentation amplifier with a programmed gain of 200. The change in the piezoresistance, $\Delta R(T)$, is directly proportional to the maximum deflection of the cantilever²⁴:

$$\Delta R(T) = 3Rz_{\max}(T) \times 10^{-6} \quad (2)$$

where $z_{\max}(T)$ is expressed in nm.

The thermally induced deflection of the cantilever is caused by the bimaterial effect which arises due to the difference in the thermal expansion coefficients of the IR coating, the metal layer, and the native silicon body of the cantilever. A reference bias voltage V_0 (equal to 9 volts in these experiments) was applied across the circuit and the voltage difference, $\Delta V(T)$, across the Wheatstone bridge circuit was digitized using a Tektronix TDS 544A digital oscilloscope or fed into a Stanford Research Systems SR850 lock-in amplifier. The measured voltage ΔV is related to the deflection of the cantilever by:

$$\Delta V(T) = \frac{3V_0}{4} z_{\max}(T) \times 10^{-6} \quad (3)$$

The experimental measurements were performed using piezoresistive microcantilevers as temperature sensors in the

configuration shown in Figure 2(a). The commercially available piezocantilever or piezolever²² was coated with $\sim 50\text{nm}$ of gold black which served as the IR absorbing material. IR radiation was then focused onto the sensor using a 2.54cm diameter IR lens with a focal length of 3.5cm and a wavelength transmission range between $0.6\text{--}15\mu\text{m}^{26}$. A Stanford Research Systems SR-540 chopper was used to modulate the IR radiation upon the detector. The sensor assembly was positioned 15cm from a soldering iron which served as the IR source. A calibrated thermocouple was attached to the IR source so that its temperature could be recorded.

The thermal power absorbed by the detector can be described as:

$$P_{\text{thermal}} = \eta \frac{dQ}{dt} = \eta t_L \left(\frac{A'_D}{2\pi L^2} \right) A_S \epsilon \sigma_{S-B} (T_S^4 - T_R^4) \quad (4)$$

where t_L is the transmission of the lens, A'_D is the effective area of the sensor, L is the distance of the detector from the source, A_S is the area of the target (IR source), ϵ is the target's emissivity, σ_{S-B} is the Stefan-Boltzmann constant ($\sim 5.67 \times 10^{-12} \text{W} \cdot \text{cm}^{-2} \cdot \text{K}^{-4}$), T_S is the temperature of the IR source, and T_R is the background temperature. In the present studies $t_L \sim 0.7$, $A'_D = 6.2 \times 10^{-4} \text{cm}^2$, $L \sim 15\text{cm}$, $A_S \sim 90\text{cm}^2$, and $18\mu\text{m}$. Using these values in Eq. (4), the absorbed thermal power (in Watts) is $P_{\text{thermal}} \sim 6.064 \times 10^{-17} [T_S^4 - (294)^4]$ (assuming that $\eta \sim 0.9$ and a measured $\epsilon \sim 0.43$ for the hot iron IR source).

The response ΔV was measured as a function of the temperature, T , of the IR source. This is plotted in Figure 3(a) along with the deflection, z_{\max} , of the piezolever and can be seen to be a monotonically increasing function of temperature. In Figure 3(b) a plot of the response of Wheatstone bridge circuit, ΔV , and the deflection, z_{\max} , of the piezolever detector as a function of the total power absorbed by the detector and it can be seen that it increases linearly with increasing power.

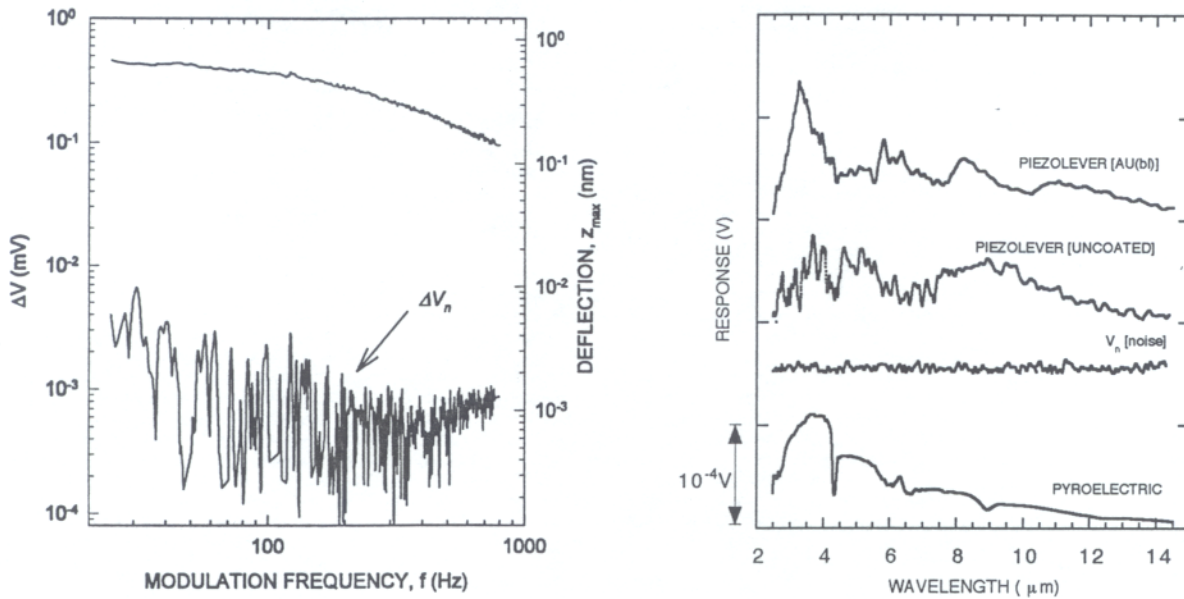


Figure 4. Left-hand-image is the response of the Wheatstone bridge detection circuit, ΔV , deflection, z_{\max} and noise ΔV_n of the piezolever as a function of the modulation frequency. Right-hand-image is the wavelength response of a gold black coated piezolever, uncoated piezolever, the noise level of the piezolever with the source blocked and the response of a pyroelectric device with its signal reduced by a factor of 500.

From the slope of this line, a deflection sensitivity of $0.125 \text{ nm}/\mu\text{W}$ is obtained. At a modulation frequency of 30 Hz , a noise equivalent power (NEP) of $\sim 70 \text{ nW}/\text{Hz}^{1/2}$ was also obtained, using $NEP = (\Delta V_n / \Delta V \sqrt{B}) \times P_{\text{thermal}}$; ΔV_n is the background noise level ($\Delta V_n \sim 10^{-6} \text{ V}$), B is the bandwidth (1 Hz).

The response of the detector was also measured as a function of the distance from an IR source. This is shown in Figure 3(c) where ΔV and z_{\max} are plotted as a function of the distance, L , between the detector and the surface of the soldering iron (IR source); L was varied from 14 cm to 35 cm . The ambient temperature was $\sim 294 \text{ K}$ and the temperature of the IR source was held at 693 K . The measured ΔV and calculated z_{\max} were found to decrease with increasing distance and followed closely an inverse square relationship with distance [see Eq. (4)] for distances larger than 15 cm .

Since the response of any thermal sensor depends on both the amount of heat falling onto the detector and the length of time it is exposed to the incoming IR radiation, we measured the response of the Wheatstone bridge circuit, ΔV , and the deflection, z_{\max} , as a function of modulation frequency of the IR radiation (Figure 4) (It should be noted that no effort has been made to separate the relative signals obtained from the bimetallic bending of the cantilever, the thermal gradient present through the cross-sectional thickness of the cantilever or the potential temperature dependent piezoresistive coefficient for these cantilevers. Ohmic heating results performed on piezoresistive cantilevers by Gimzewski *et al.*

have shown that there is a definite bending component present¹⁸). It can be seen that the detector response (and the deflection of the cantilever) decreases with increasing modulation frequency. The temporal response of the temperature sensor was also determined by measuring ΔV as a function of time. The microcantilever was found to exhibit two thermal response times due to the incoming IR radiation; a time $\tau_1^{th} < 1 \text{ ms}$ and a time τ_2^{th} that is somewhat longer ($\sim 10 \text{ ms}$). These two time constants are attributed to the two different thermal dissipation lengths present for these cantilevers - τ_1^{th} for the time needed to dissipate through the thickness of the lever and τ_2^{th} for the dissipation along the length of the beam structure. Additionally, measurements of the IR wavelength response of coated [gold-black - Au(bl)] and uncoated piezolevers are shown in Figure 4. The spectral response was made with a blackbody radiator ($T=1170 \text{ K}$) from a Miran 80 - Gas Infrared Analyzer over a wavelength region between $2.5 \mu\text{m}$ and $14.6 \mu\text{m}$. It is clearly evident when comparing the coated and uncoated piezolevers, there is a considerable enhancement of the coated levers response in the wavelength range of $2.5-4.5 \mu\text{m}$. Additionally, for these same two levers, there is a relatively similar characteristic response above $8 \mu\text{m}$ in wavelength. Noise levels for the piezoresistive levers is also shown in this figure. The lowest curve in this figure shows the response of a pyroelectric detector used by the Miran Analyzer. For display purposes, the response scale of this curve has been reduced by a factor of 500. This might inaccurately be an indication of the relative insensitivity of the piezoresistive

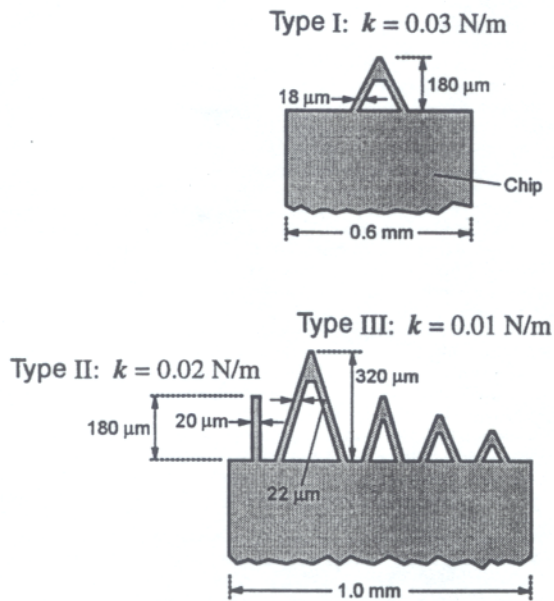


Figure 5. Schematic view of the $0.6\mu\text{m}$ thick Si_3N_4 microcantilevers used for evaluation of thermal response. Note that results from only the two left-most microcantilevers (out of five total) on the lower chip are presented.

sensor compared to the pyroelectric device, but when taking into account the relative areas of the devices, the signal from the piezoresistive sensor is approximately 80 times larger than that of the pyroelectric device.

These findings demonstrate that small changes in temperature induce deflections of the microcantilever correspond to measurable changes in the piezocantilever resistance. It should be noted that these commercially available piezolevers have been designed to be minimally sensitive to changes in temperature so as to reduce the noise and interference in scanning probe microscopy applications. Therefore, the temperature sensitivity of the piezolever could be further improved by optimizing its shape, IR absorbing coating and thermal isolation⁶.

Optical Deflection Monitoring

Cantilever deflections can also be monitored using an optical technique similar to that used in atomic force microscopy as shown in Figure 2(b). Microcantilevers were mounted in a holder (from Digital Instruments) designed for tapping mode AFM, which secured the base of the microcantilever against a small piezoelectric transducer; this chip holder was then mounted on a three-axis translation stage to facilitate fine adjustment of the microcantilever relative to the rest of the experimental apparatus. Collimated optical radiation from a diode laser was used to evenly illuminate the mounted microcantilever (pump wavelength of 786nm , beam diameter of 6mm , centered on the tip of cantilevers $180\text{--}320\mu\text{m}$ in length). Output of this excitation source was modulated sinusoidally at frequencies ranging from DC to 100kHz , with peak powers ranging from 0 to 18.5mW (0 to $65\text{mW}/\text{cm}^2$).

This configuration provided a flexible, easily controlled test system for quantifying microcantilever response to optical energy^{11,27}. All measurements were conducted at ambient temperature and atmospheric conditions.

A second laser was used in a probe configuration to monitor bending. A helium-neon laser (or HeNe, delivering 3mW at 633nm) was focused onto the tip of the microcantilever using a $10\times$ microscope objective; to minimize heating of the tip by the probe laser, optical power was reduced by placing a neutral density filter with an optical density of 1.0 between the probe laser and the objective. A dual element photodiode displacement detector was used to collect the reflected probe beam [position detectors PD_1 and PD_2 in Figure 2(b)]; a 1nm bandpass filter centered at 633nm was placed in front of the detector to block scattered light from the pump laser. The difference signal from the detector pair as the cantilever tip changed position ($[(PD_1 - PD_2)] / [(PD_1 + PD_2)]$) was used to measure the displacement, d . This signal was directly digitized and stored, or sent to a lock-in amplifier (SR850, Stanford Research Systems) for signal extraction and averaging. The lock-in amplifier was also used to control modulation frequency and output level of the pump laser.

Optical response characteristics of three different types of commercially available AFM probe tips were evaluated. These microcantilevers are shown schematically in Figure 5 as well as in the scanning electron micrograph of Figure 1. Microcantilevers typically come from the manufacturer attached to a large rectangular chip (ca. 1mm wide \times 3mm long \times 1mm

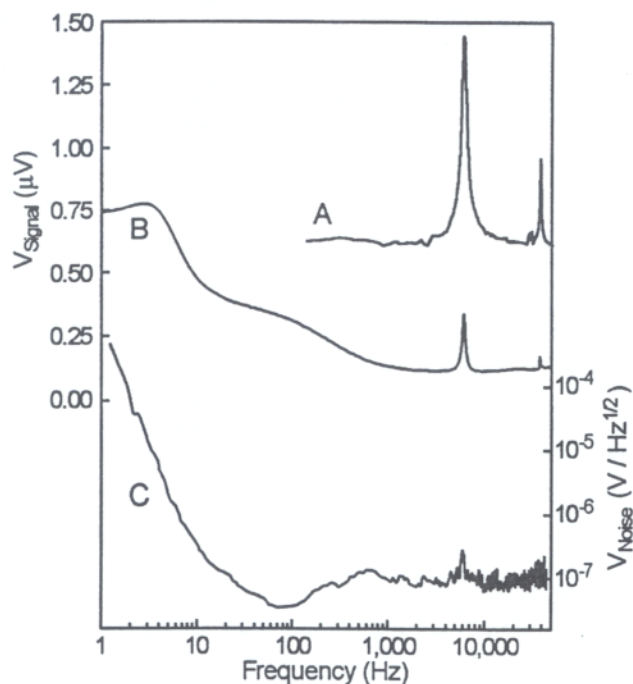


Figure 6. Mechanical and optical excitation spectra for a Type III microcantilever. Response to frequency swept mechanical excitation is given in spectrum 'A'; similar results for optical excitation are shown in spectrum 'B'. Optical excitation was effected using a sinusoidally modulated pump laser at 786 nm. Spectrum 'C' shows noise response when the pump laser is operated in a dc mode. Fundamental mechanical resonance at 6.2 kHz and higher-order resonance at 37 kHz are evident for both optical and mechanical excitation.

thick) that is used to facilitate manipulation and mounting, and all those evaluated in this work were used as received. The microcantilevers used were: a triangular silicon nitride Si_3N_4 microcantilever (labeled "I" in Figure 5, with a length of 180 μm , a width of 18 μm and a bending force constant $k \sim 0.3 N/m$, from Park Scientific); a rectangular silicon nitride microcantilever (labeled "II", 200 μm in length and 20 μm in width, bending force constant $k \sim 0.2 N/m$, Park Scientific); and a triangular silicon nitride cantilever (labeled "III", which was 320 μm long and 22 μm wide, with a bending force constant $k \sim 0.1 N/m$, Park Scientific). Each was 0.6 μm thick. The Type I cantilever was coated with 50 nm of aluminum on one side to see how this would affect its optical response characteristics; Types II and III were used as received from the manufacturer, with a gold/chromium film uniformly covering one side (2–3 nm of chromium followed by 40 nm of gold).

An essential aspect of any scheme for micromechanical optical detection is the ability to sensitively detect physical changes resulting from thermal stress, since this directly affects the sensitivity and precision in measurement of temperature change or thermal flux. As an initial evaluation of the ability to detect optically-induced bending of a microcantilever, each of the three types of microcantilever were subjected to both mechanical and optical excitation, and their response measured as a function of excitation frequency. Mechanical excitation was achieved by driving the piezoelectric element in the AFM

chip holder with the reference signal from the lock-in amplifier; such mechanical excitation spectra are helpful in locating resonance frequencies for allowed microcantilever bending modes. Optical excitation spectra were obtained by modulating the pump laser with the lock-in reference signal. Typical response spectra for a triangular microcantilever (Type III) are shown in Figure 6. The mechanical spectrum (curve "A") shows two resonances, at 6 kHz and 38 kHz, attributable to the fundamental transverse resonance and a higher-order resonance (possibly torsional bending), respectively. The optical spectrum (curve "B") shows similar resonance features, although with somewhat different relative intensities; a large, broadband response is also noted at low frequencies. No synchronous oscillatory response was noted when the microcantilever was excited with constant dc laser power (curve "C"). Similar response was noted under these conditions for the other two microcantilevers.

Figure 6(B) shows that microcantilever response to optical input decreases rapidly for frequencies above 10 Hz, but that mechanical resonance is still observed even at frequencies well above 10 kHz. In fact, the Type I and II microcantilevers exhibited strong optical resonance at frequencies of 17 kHz and 14 kHz, respectively; these modes correspond to the fundamental transverse resonances for the microcantilevers. Such resonant response demonstrates that reversible heating and bending of the cantilever occurs as a result of optical

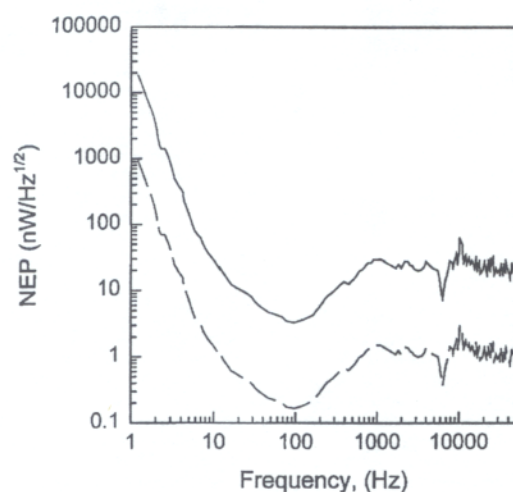


Figure 7. Noise equivalent power (NEP) as a function of modulation frequency for a Type III Si_3N_4 microcantilever. Optical excitation at 785nm , utilizing bimetallic bending induced in a gold/chromium film. Dashed curve represents the NEP when the reflectivity of the cantilever is taken into account.

excitation, producing mechanical vibration. These resonances also have quality factors that are identical to their mechanically-driven counterparts, confirming that optically-pumped mechanical vibration is occurring.

The rapid roll-off in response observed in Figure 6(B) is attributed to thermal equilibration of the cantilever at high modulation frequencies. Because the cantilever must dissipate heat between laser pulses, the finite thermal conductivity of its legs limits the rate at which heat from these thermal impulses can be transferred out of the microcantilever and into the support structure (the chip); thus, as modulation frequency is increased and the microcantilever approaches thermal equilibrium, changes in thermal stress as a function of time approach zero. Thermal dissipation most likely will be dominated by heat transfer through the cantilever legs instead of through the air due to the large difference in thermal conductivities between these two media.⁵

In order to evaluate the role of optical reflectivity (or thermal absorptivity) on microcantilever response, a silicon nitride microcantilever (the Type I specimen) was coated on one side with a thin layer of aluminum; note that the manufacturer's gold/chromium film was removed prior to aluminum deposition. This produced a microcantilever that had a nearly transparent body that was highly reflective to the pump laser on the aluminum coated side (reflectivity, $R \sim 0.95$ at 786nm), but slightly less reflective on the uncoated side (due to absorption of the pump radiation upon transmission through the Si_3N_4 cantilever body). As expected, the resonant frequency of this cantilever was found to be 17kHz . However, when the uncoated side of the microcantilever was illuminated (reverse geometry), the magnitude of bending response at all frequencies increased by about 20% in comparison to normal illumination on the reflective side. We believe this difference is attributable to increased absorption of the pump beam upon transmission

through the Si_3N_4 material, resulting in more effective transduction of optical energy into thermal heating of the microcantilever. While this simple experiment demonstrates that sensitivity can be improved by increasing absorption of impinging optical radiation, it is obvious that to optimize the method further suitable optically absorbing coatings are needed (such as carbon black, gold black, or other broadband absorbers). Unfortunately, such materials were not available for this study.

Photometric response was further characterized by measuring microcantilever response at various modulation frequencies and optical pump levels (Figures 7 and 8, and Table I). For the Type III Si_3N_4 microcantilever, we estimate a noise equivalent power (NEP) of 3.5nW/Hz at 20Hz , with a bandwidth, B , of 0.26Hz . The specific detectivity, D^* , is equal to $3.6 \times 10^7 \text{cm} \cdot \text{Hz}^{1/2}/\text{W}$ under these conditions, where $D^* = (A^{1/2} \Delta V) / (\Delta V_n P)$ and A is the area of the detector element. Note that the characteristics of this initial, unoptimized microcantilever compare quite favorably with some room temperature technologies currently under development, including indium antimonide photoconductors ($NEP = 5\text{nW}$ at 500Hz)²⁸, but are not yet competitive with silicon microbolometers ($NEP = 5\text{pW/Hz}$, $NETD = 40\text{mK}$ at 30Hz)²⁹ or pyroelectric devices ($NEP = 8\text{pW/Hz}$, $D^* = 3.5 \times 10^8 \text{cm} \cdot \text{Hz}^{1/2}/\text{W}$)³⁰. However, in contrast to these highly optimized examples, several simple improvements to our microcantilever system are obvious that could improve performance dramatically. For instance, since the metal coating on the tested cantilevers is highly reflective at the pump wavelength (for gold, $R > 98\%$ at 785nm), use of an improved

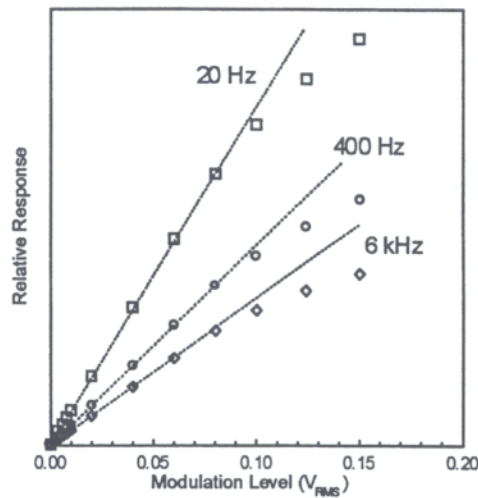


Figure 8. Photometric response for a typical microcantilever (Type III) at various optical pump levels using excitation at 20Hz, 400Hz and 6kHz.

absorptive coating (such as gold black, $R < 2\%$) could improve NEP in this example to $< 75 \text{ pW}$. Furthermore, the observed detection limits appear to be determined by readout noise in our optical detection circuit. We believe that with careful design of this circuitry, performance could be substantially improved. Finally, response of the microcantilevers was extremely linear (with a correlation coefficients, $r_2 > 0.99995$) for all but the highest test levels; roll-off in measured response for very high laser modulation levels is an artifact of our method for modulating the pump laser, which exhibited a reduced depth of modulation at high drive levels.

Conclusions

A novel uncooled infrared detector using microcantilever is demonstrated. A noise equivalent temperature difference, $NETD = 90 \text{ mK}$ was measured. When uncoated microcantilevers were irradiated by a low-power diode laser ($\lambda = 786 \text{ nm}$) the

noise equivalent power, NEP , was found to be $3.5 \text{ nW}/\sqrt{\text{Hz}}$ which corresponds to a specific detectivity, D^* , of $3.6 \times 10^7 \text{ cm}\cdot\sqrt{\text{Hz}}/\text{W}$ at a modulation frequency of 20 Hz with numbers of $173 \text{ pW}/\sqrt{\text{Hz}}$ and $7.18 \times 10^8 \text{ cm}\cdot\sqrt{\text{Hz}}/\text{W}$ being obtained for NEP and D^* , respectively, when the reflectivity of the cantilever is considered. The sensitivity of detection can be further improved by optimization. For example, while the microcantilevers employed here were optimized for standard AFM applications, vastly improved detectors could be produced by making relatively simple changes in the materials and geometries used in microcantilever fabrication. It is possible to design microcantilevers with much smaller force constants by varying the geometry of the cantilever, and in contrast to the devices used in this study, cantilevers with force constants as small as 0.006 N/m are now commercially available. Since the fundamental mechanical resonance frequency of a microcant-

Table I. Photometric response at 785nm for a gold/chromium coated Si_3N_4 microcantilever (Type III). Data at 6.02kHz was obtained at the mechanical of the microcantilever. (# The numbers in the parenthesis are those obtained when the reflectivity of the cantilever is taken into account.).

Optical Modulation Frequency (Hz)	Detector Time Constant (ms)	V_{signal} (μV)	V_{noise} (μV)	NEP ($\text{nW}/\text{Hz}^{1/2}$)	D^* ($\text{cm}\cdot\text{Hz}^{1/2}/\mu\text{W}$)
6020	300	307.1	0.585	13.1(0.655)#	9.48(189.6)
	30	305.3	1.76	12.5(0.625)	9.91(198.2)
	1	305.5	9.46	12.3(0.615)	10.10(202)
400	300	223.2	0.196	6.03(0.302)	20.06(401.2)
	30	221.1	0.691	6.78(0.339)	18.30(366)
	10	226.3	1.19	6.59(0.330)	18.80(376)
20	300	528.2	0.266	3.46(0.173)	35.90(718)

iver is proportional to \sqrt{k} , reductions in force constant can be used to bring resonance into ranges compatible with mechanical chopping frequencies. It is also clear that the coatings applied to the cantilever are at least as important as the composition of the cantilever itself. For example, metals with higher thermal expansion coefficients such as films of Al, Zn, Pb, or In could be used to increase the thermally-induced bending of the cantilever. Coating the surface of the cantilever with high emissivity materials (such as gold black) can also enhance IR response.

Since microcantilever spectral response can be easily tailored through the application of specific absorptive coatings, choice of material for fabrication of the microcantilever can be determined primarily by the requirements of the manufacturing process. This means that microcantilevers can be fabricated using standard semiconductor methods and materials, and as a consequence could be mass produced at very low cost. Hence, two-dimensional cantilever arrays based on the technology described here could become very competitive with existing technologies due to their inherent simplicity, high sensitivity, and rapid response to optical radiation. While the optical readout method is useful with single element designs, practical implementation of microcantilever arrays may require the use of other readout methods, such as piezoresistance. Fortunately, the microcantilever technology's compatibility with a variety of readout methods also affords tremendous flexibility to potential system designers.

Acknowledgments

Research sponsored by U.S. Department of Energy under contract DE-AC05-96OR22464 with Lockheed Martin Energy Research Corp. The authors wish to acknowledge the support of the ORNL Seed Money Program. The authors would like to thank Dr. Isidor Sauers for the use of his Miran 80 - Gas Infrared Analyzer. The efforts of P.I. Oden were supported, in part, by an appointment to the Alexander Hollaender Distinguished Postdoctoral Fellowship Program sponsored by the U.S. Department of Energy, Office of Health and Environmental Research, and administered by the Oak Ridge Institute for Science and Education. P.G. Datskos wishes to acknowledge the support of the ~~National Science Foundation under the SBIR award DM2-9460929~~ to Consultec Scientific, Inc.

References

1. R. J. Kayes, Editor "Optical and Infrared Detectors," *Topics in Applied Physics*, Volume 19, Springer Verlag Berlin (1977).
2. P. Howard, J. Stevens, C. Rau, R.J. Herring, and R.A. Wood, *Infrared Technology XXI*, SPIE Vol. 2552, 60, July 1995.
3. E. L. Dereniak, G. D. Boreman, "Infrared Detectors and Systems", Wiley Series in Pure and Applied Optics, Wiley and Sons, New York (1996).
4. J. M. Lloyd, "Thermal Imaging Systems", Plenum Press, New York (1975).
5. Jacob Fraden, "AIP Handbook of Modern Sensors - Physics, Designs and Applications", AIP Press, New York (1993).
6. E. Meyer, J. K. Gimzewski, Ch. Gerber and R. R. Schlittler, "Micromechanical calorimeter with picojoule sensitivity", in *Ultimate Limits of Fabrication and Measurement*, Proceedings

- of the NATO ASI Series E: Applied Science, Vol. 292, M. E. Welland and J. K. Gimzewski (eds.) p. 89 (1995).
7. J.R. Barnes, R.J. Stephenson, C.N. Woodburn, S. J. O'Shea, M.E. Welland, T. Rayment, J. K. Gimzewski, Ch. Gerber, *Rev. Sci. Instrum.*, **65**, 3793 (1994); J. R. Barnes, R. J. Stephenson, M. E. Welland, Ch. Gerber, J. K. Gimzewski, *Nature*, **372**, 79 (1994).
8. O. Nakabeppu, M. Chandrachood, Y. Wu, J. Lia, and A. Majumdar, *Appl. Phys. Lett.*, **66**, 694 (1995).
9. N. Umeda, S. Ishizaki, and H. Uwai, *J. Vac. Sci. Technol.*, **B9**, 1318 (1991).
10. M. Allegrini, C. Astoli, P. Baschieri, F. Dinneli, C. Frediani, A. Lio, and T. Mariani, *Ultramicroscopy*, **42-44**, 371 (1992).
11. O. Marti, A. Ruf, M. Hipp, B. Bielefeldt, J. Colchero, and J. Mlynek, *Ultramicroscopy*, **42-44**, 345 (1992).
12. J. Mertz, O. Marti, and J. Mlynek, *Appl. Phys. Lett.*, **62**, 2344 (1993).
13. J. K. Gimzewski, Ch. Gerber, E. Meyer, and R. R. Schlittler, *Chem. Phys. Lett.*, **217**, 589 (1994).
14. T. Thundat, R. J. Warmack, G. Y. Chen, and D. P. Allison, *Appl. Phys. Lett.*, **64**, 2894 (1994).
15. E. A. Wachter, T. Thundat, P. G. Datskos, P. I. Oden, S. L. Sharp, and R. J. Warmack, *Rev. Sci. Instrum.* (submitted).
16. G. Y. Chen, T. Thundat, E. A. Wachter, R. J. Warmack, *J. Appl. Phys.*, **77**, 3618 (1995).
17. P.G. Datskos, P.I. Oden, T. Thundat, E.A. Wachter, R.J. Warmack and S.R. Hunter, *Appl. Phys. Lett.* (submitted).
18. J. K. Gimzewski, Ch. Gerber, E. Meyer, and R. R. Schlittler, "Micromechanical Heat Sensor: Observation of a Chemical Reaction, Photon and Electrical Heat Pulses", in *Forces in Scanning Probe Methods*, Proceeding of the NATO ASI, H.-J. Güntherodt, D. Anselmetti, and E. Mayer (eds.) p. 123 (1995).
19. D. Sarid, *Scanning Force Microscopy*, Oxford University Press, New York, (1991).
20. "Investigations of the Reconstructed Gold Surface with Electrochemical Scanning Probe Microscopy" - PhD. dissertation, Patrick Ian Oden, Arizona State University Physics Department (1993).
21. P.I. Oden, N.J. Tao and S.M. Lindsay, *J. Vac. Sci. Technol.* **B11(2)**, 137 (1993).
22. Commercial versions available from Park Scientific, Sunnyvale, CA.
23. W. C. Young, *Roark's Formulas for Stress and Strain*, Sixth ed., McGraw Hill, New York, pp. 118 (1989).
24. M. Tortonese, R. C. Barrett, and C. F. Quate, *Appl. Phys. Lett.*, **62**, 834 (1993).
25. F. J. Giessibl and B. M. Tafas, *Rev. Sci. Instrum.*, **65**, 1923 (1994).
26. Oriel Co., Model 43402 AMTIR-1 lens.
27. M. Allegrini, C. Ascoli, P. Baschieri, F. Dinelli, C. Frediani, A. Lio, T. Mariani, *Ultramicros.*, **42-44**, 371 (1992).
28. R. Anton, E.L. Dereniak, and J. Garcia, *Infrared Technology XXI*, SPIE Vol. 2552, 592, July 1995.
29. N. Butler, R. Blackwell, R. Murphy, R. Silva, and C. Marshall, *Infrared Technology XXI*, SPIE Vol. 2552, 583, July 1995.
30. S. Fujii, T. Kamada, S. Hayashi, Y. Tomita, R. Takayama, T. Hirao, T. Nakayama, and T. Deguchi, *Infrared Technology XXI*, SPIE Vol. 2552, 612, July 1995.

000 NAV JBIE